



UDC 666.3

## STUDY OF VANADATE UNITS USING DENSITY FUNCTIONAL THEORY: ELECTRONIC PROPERTIES AND REACTIVITY

Abdelahad EL Addali<sup>1\*</sup>, Abdellah EL Boukili<sup>2</sup>, Lahcen Boudad<sup>2</sup>, Hamid Zouihri<sup>3</sup>, M'hamed Taibi<sup>2</sup>,  
Taoufiq Guedira<sup>1</sup>

<sup>1</sup> Ibn Tofail University in Kenitra, Laboratory of Organic Chemistry, Catalysis and Environment, (LOCCE), Faculty of Sciences, Kenitra, (F.S.K), Morocco.

<sup>2</sup> Mohammed V University in Rabat, Centre Sciences des Matériaux, Laboratoire de Physico-Chimie des Matériaux Inorganiques et Organiques (LPCMIO), Ecole Normale Supérieure, Rabat, Morocco.

<sup>3</sup> Moulay Ismail University in Meknès, Materials Membranes and Nanotechnology Laboratory, Faculty of Sciences, Meknès, BP: 11201 Zitoune, Morocco.

Received 11 January 2024; accepted 26 March 2024; available online 10 July 2024

### Abstract

The vanadate units have been theoretically investigated through density functional theory calculations. The global reactivity indices have been optimized. The obtained results revealed that the (Q<sub>0</sub>) [VO<sub>4</sub>]<sup>3-</sup> unit shows an electron-donor character, while the units Q<sub>1</sub>, Q<sub>2</sub>, and Q<sub>3</sub> units are evidenced to exhibit an electron-acceptor feature. The transition from one unit to another is found to be accompanied by an increase in the number of bridging oxygen atoms, in accordance with the highlighted changes in Mulliken charges. Moreover, the analysis of the optimized electrostatic potential surfaces indicated a higher likelihood of nucleophilic attacks on the vanadium atoms. Predictions for infrared and Raman spectra were also conducted, revealing changes in symmetric and asymmetric vibrational bands as the number of bridging oxygen atoms varied. Additionally, Fukui indices were employed to identify the preferred sites for the electrophilic attack within the (Q<sub>0</sub>) [VO<sub>4</sub>]<sup>3-</sup> unit on the Q<sub>1</sub>, Q<sub>2</sub>, and Q<sub>3</sub> vanadate units.

**Keywords:** Vanadate units; DFT; Global reactivity indices; electrostatic potential; nucleophilic; FUKUI indexes.

## ДОСЛІДЖЕННЯ ВАНАДАТНИХ СПЛУК З ВИКОРИСТАННЯМ ТЕОРІЇ ФУНКЦІОНАЛУ ГУСТИНИ: ЕЛЕКТРОННІ ВЛАСТИВОСТІ ТА РЕАКЦІЙНА ЗДАТНІСТЬ

Абделахад Ель Аддалі<sup>1</sup>, Абделла Ель Букілі<sup>2</sup>, Лахсен Будада<sup>2</sup>, Хамід Зуїхрі<sup>3</sup>, М'хамеде Тайбі<sup>2</sup>,  
Тауфік Гuedіра<sup>1</sup>

<sup>1</sup> Університет Ібн Тофайла в Кенітрі, Лабораторія органічної хімії, каталізу та навколишнього середовища (LOCCE), Факультет наук, Кенітра, Марокко.

<sup>2</sup> Університет Мохаммеда V в Рабаті, Центр наук про матеріали, Лабораторія фізико-хімії неорганічних і органічних матеріалів (LPCMIO), Вища нормальна школа, Рабат, Марокко.

<sup>3</sup> Університет Мулая Ісмаїла в Мекнесі, Лабораторія мембранних матеріалів та нанотехнологій, природничий факультет, Мекнес, BP: 11201 Зітун, Марокко.

### Анотація

За допомогою розрахунків теорії функціоналу густини теоретично досліджені ванадатні агрегати. Оптимізовано індекси глобальної реактивності. Одержані результати показали, що агрегат (Q<sub>0</sub>) [VO<sub>4</sub>]<sup>3-</sup> має електронодонорний характер, в той час як агрегати Q<sub>1</sub>, Q<sub>2</sub> і Q<sub>3</sub> – електроноакцепторний. Встановлено, що перехід від одного елемента до іншого супроводжується збільшенням кількості зв'язуючих атомів кисню, відповідно до виявлених змін у зарядах Маллікена. Крім того, аналіз оптимізованих поверхонь електростатичного потенціалу вказує на більшу ймовірність нуклеофільних атак на атоми ванадію. Було також проведено прогнозування інфрачервоних і комбінаційних спектрів, яке виявило зміни в симетричних і несиметричних коливальних смугах під час зміни кількості зв'язуючих атомів кисню. Крім того, для визначення переважних ділянок для електрофільної атаки в межах (Q<sub>0</sub>) [VO<sub>4</sub>]<sup>3-</sup> на ванадатні одиниці Q<sub>1</sub>, Q<sub>2</sub> і Q<sub>3</sub> використано індекси Фукуї.

**Ключові слова:** Ванадатні одиниці; DFT; індекси глобальної реактивності; електростатичний потенціал; нуклеофільність; індекси FUKUI.

\*Corresponding author: e-mail: [hioaddali@gmail.com](mailto:hioaddali@gmail.com)

© 2024 Oles Honchar Dnipro National University;

doi: 10.15421/jchemtech.v32i2.296585

## Introduction

Owing to their interesting combination of physical and chemical properties, vanadium-based materials have emerged as a fascinating and versatile class of substances with a wide range of applications in various fields of science and industry. These materials have found essential roles in metallurgy [1], catalysis [2], energy storage [3], and more [4; 5]. In the context of metallurgy, vanadium alloys offer improved mechanical properties and corrosion resistance, making them vital components in aerospace and structural applications [6]. Moreover, vanadium is a key player in the world of catalysis, where its compounds enable various chemical transformations and the production of chemicals and fuels [7]. In the realm of energy storage, vanadium-based redox flow batteries have gained attention due to their promising advantages [8]. These materials are also of great interest in the development of next-generation electronics and nanotechnology, offering potential breakthroughs in the miniaturization and performance of devices [9].

The optical properties of vanadate glasses have also received significant attention in comparison to their electrical properties. Indeed, there have been some investigations conducted in the infrared spectrum, which have involved the study of the absorption edge of these glasses. Notably, many studies have been conducted on the lower-energy region of the absorption edge of crystalline  $V_2O_5$ , revealed to adhere to Urbach's rule. Also, several studies have examined the structural characteristics of vanadate glasses [10–12]. It has been noted that the structural arrangement of these glasses is influenced by both the types of network formers and modifiers. Furthermore, there is a distinct interest in expanding our comprehension of the structure of these glass materials and obtaining a more accurate representation of their short-range atomic arrangement. The vanadate glasses are materials with a structure formed by vanadium tetrahedrons  $VO_4$  that fit together by forming bonds between each other. This class of glasses can also be described as a three-dimensional cross-linked network of vanadate tetrahedral denoted  $Q_i$ , where it refers to the number of neighboring tetrahedra linked through a common oxygen bridge [13–14].

There are four possible structural entities of the  $VO_4$  tetrahedron, each denoted as follows:

-  $Q_0$ : ( $[VO_4]^{3-}$ ) consisting of four non-bridging oxygen atoms (NBO).

-  $Q_1$ : ( $[V_2O_7]^{4-}$ ) where Two tetrahedral  $[VO_4]$  are linked together by a common oxygen atom, which acts as bridging oxygen (BO), resulting in the formation of ( $[V_2O_7]^{4-}$ ) molecule.

-  $Q_2$ : ( $[V_3O_9]^{3-}$ ) consisting of three tetrahedral  $[VO_4]$  units interconnected through oxygen bridges to form the  $[V_3O_9]^{3-}$  structural entity.

-  $Q_3$ : ( $[V_4O_{10}]^0$ ) where four tetrahedral  $[VO_4]$  are connected through oxygen bridges to create the  $[V_4O_{10}]^0$  structural unit.

In this paper, we conducted a theoretical study of many vanadate units, through the DFT calculation method using the B3LYP function associated with the 6-311G base [15]. In addition to optimizing the geometry of these vanadate units, we delve into their chemical reactivity through a comprehensive analysis of various global reactivity indices. These include HOMO-LUMO energy gaps, ionization potential, electronic affinity, electrophilicity index, chemical potential, hardness, and softness. This study also explored the charges, dipole moments, distances, angles, and optimized surfaces of molecular electrostatic potential. Moreover, the explored vibrational frequencies highlighted both symmetric and asymmetric vibrations in the chains, based on the computed IR and Raman spectra. Furthermore, within the scope of this study, we analyzed the reactivity of the  $Q_1$ : ( $[V_2O_7]^{4-}$ ),  $Q_2$ : ( $[V_3O_9]^{3-}$ ), and  $Q_3$ : ( $[V_4O_{10}]^0$ ) vanadates with the  $Q_0$  ( $[VO_4]^{3-}$ ) unit ion to generate a stable structured product. This research also aims to identify the electrophilic sites that promote this interaction, thus facilitating the establishment of a stable framework.

## Experimental

*Computational details.* All the reported calculations have been conducted by the Gaussian 09 software program based on the DFT/RB3LYP density functional theory method and employing a 6-311G basis set. The stability of vanadate units has been meticulously optimized by considering variables such as charges,  $E_{HOMO}$  and  $E_{LUMO}$  molecular orbital energies, electrostatic potentials, and global reactivity indices.

The ionization energy or ionization potential (IP), defined as the minimum energy necessary to extract an electron from an atom or molecule, has been calculated by the following formula:

$$IP \approx -E_{HOMO} \quad (1)$$

The electron affinity (EA), representing the energy released when an electron is captured, has been calculated using the following formula:

$$AE \approx -E_{\text{LUMO}} \quad (2)$$

The chemical potential is a variable related to both electrophilicity (attraction of electrons) and nucleophilicity (release of electrons). This chemical potential is calculated as follows [16; 17]:

$$\mu = \frac{-(IP + AE)}{2} \quad (3)$$

The chemical hardness ( $\eta$ ) is a parameter that serves as an indicator of the molecular system stability. It quantifies the system's ability to resist electron transfer, encompassing both the gain and loss of electrons. The chemical hardness has been calculated via the equation [16; 18]:

$$\eta = \frac{IP - AE}{2} \quad (4)$$

The electrophile index ( $\omega$ ), denoted as  $\omega$ , serves as a measure of the capacity of a molecular system to form strong bonds with a nucleophilic partner through electron transfer. A higher value of  $\omega$  reflects a greater electrophilic nature in the system. The calculation formula for the overall electrophile index is as follows [17; 18]:

$$\omega = \frac{\mu^2}{2\eta} \quad (5)$$

The softness (S), which characterizes the capability of an atom or molecule to retain an electric charge, is calculated using the formula as defined in references [16; 17]:

$$S = \frac{1}{\eta} \quad (6)$$

## Results and discussion

Vanadium remains one of the most studied transition elements in oxidation catalysis, owing to its reducible nature, facile inter-conversion between its stable high oxidation states, and its ability to structure within oxides of different stoichiometries exhibiting various site geometries [19–21].

*The geometry optimization.* The geometry optimization of isolated vanadate units with their charges is illustrated in Fig. 1. The optimization procedure involved visual assessments and the estimation of approximate charges within the GAUSSIAN 09 W software. The resulting structural parameters are listed in Table 1.

Table 1

Calculated interatomic distances and angles of the Q<sub>0</sub>, Q<sub>1</sub>, Q<sub>2</sub> and Q<sub>3</sub> vanadate units for the optimized structures

		Q <sub>0</sub>	Q <sub>1</sub>	Q <sub>2</sub>	Q <sub>3</sub>
Lengths (Å) (±0.001Å)	V – O <sub>NBO</sub>	1.757	1.719	1.658	1.525
	V – O <sub>BO</sub>	-----	1.872	1.826	1.776
	V – O – V	-----	179.92	135.35	124.86
Angles (°) (±0.01°)	O <sub>NBO</sub> – V – O <sub>NBO</sub>	109.47	108.11	108.48	-----
	O <sub>NBO</sub> – V – O <sub>BO</sub>	-----	110.79	110.93	117.16
	O <sub>BO</sub> – V – O <sub>BO</sub>	-----	-----	104.64	100.79

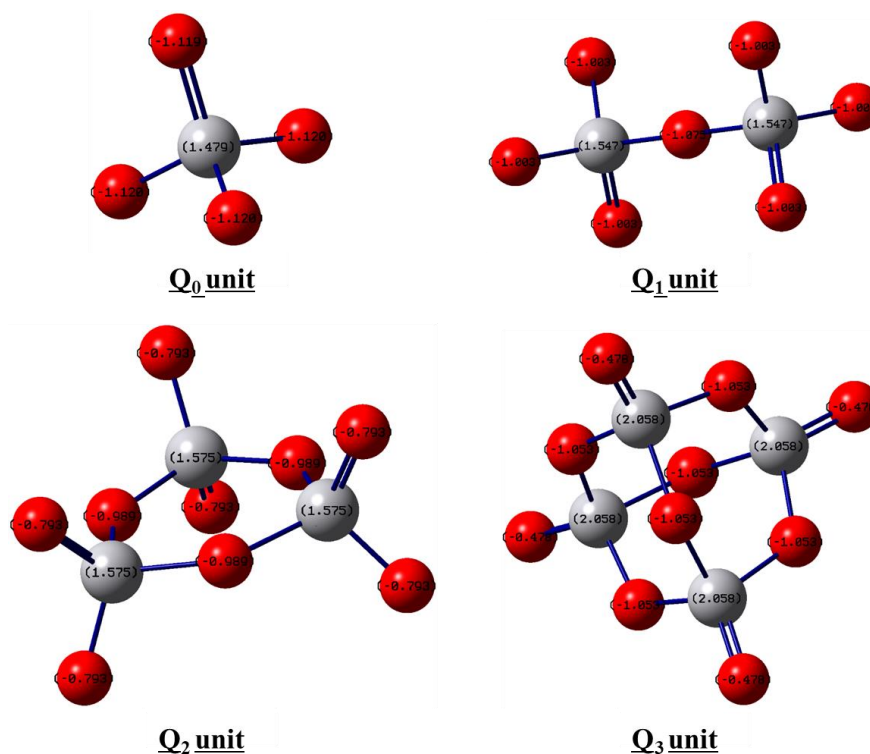


Fig. 1. Mulliken charges of the optimized Q<sub>0</sub>, Q<sub>1</sub>, Q<sub>2</sub>, and Q<sub>3</sub> units

Analysis of Fig. 1 reveals that the increase in the number of bridging oxygen atoms induces an increase in positive charges on vanadium atoms and negative charges on non-bridging oxygen atoms (NBO). The electron density of positive charges is concentrated on the vanadium atom, while the negative charges are concentrated on the non-bridging oxygen atoms NBO. The calculated interatomic distances and angles for these different units are listed in Table 1. It is noticed that the vanadium cation  $V^{5+}$  is placed in the middle of the almost perfect tetrahedron with an angle O-V-O of  $109.47^\circ$ , closely approximating the ideal value ( $109.5^\circ$ ). For the  $Q_1$  structural unit, it can be noticed that the V- $O_{BO}$  bond length has a value of  $1.872 \text{ \AA}$ , which is higher than the V- $O_{NBO}$  bond having a value of  $1.719 \text{ \AA}$ . Moreover, the two vanadium atoms and the bridging oxygen are found to be aligned as the two neighboring tetrahedral units are connected at an angle of  $179.92^\circ$ . Furthermore, the tetrahedral angle  $O_{NBO}$ -V- $O_{NBO}$  is about  $108.11^\circ$ , which is slightly lower than the tetrahedral angle of  $Q_0$  where the angle is  $109.47^\circ$ . This implies a higher tetrahedral distortion due to the V- $O_{BO}$  bond distance

diminution. For the  $[V_3O_9]^{3-}$  unit with  $Q_2$  notation, the tetrahedral  $VO_4$  units are connected through two bridging oxygens, with V- $O_{NBO}$  and V- $O_{BO}$  distances of  $1.658 \text{ \AA}$  and  $1.826 \text{ \AA}$ , respectively. Besides, the value of the V-O-V angle is revealed to be about  $135.35^\circ$  reflecting the onset of further decrease of this angle. Furthermore, one observes a slight increase in the value of the  $O_{NBO}$ -V- $O_{NBO}$  angle to about  $108.48^\circ$  owing to the distortion of the tetrahedral  $[VO_4]$ . For the  $Q_3$  unit, the V- $O_{NBO}$  and V- $O_{BO}$  distances decline to  $1.525 \text{ \AA}$  and  $1.776 \text{ \AA}$ , respectively. The tetrahedra are found to be connected at an average angle of  $100.79^\circ$ , reflecting a notable deviation from the equilibrium geometry.

*Study of global reactivity.* Table 2 groups the computed values of HOMO and LUMO energies, energy difference  $\Delta E$ , chemical potential, softness, chemical hardness, electrophilic index, and dipole moment for the different studied vanadate units. According to the molecular orbital theory due to interactions between HOMO-LUMO, the  $\pi$ - $\pi^*$  transitions are observed in transition states.

Table 2

**HOMO and LUMO energies, energy difference  $\Delta E$ , chemical potential, softness, chemical hardness, electrophile index, and dipole moment of the  $Q_0$ ,  $Q_1$ ,  $Q_2$ , and  $Q_3$  units.**

Unit	$E_{HOMO}$ (eV)	$E_{LUMO}$ (eV)	$\Delta E$ (eV)	$\eta$ (eV)	$S$ ( $eV^{-1}$ )	$\mu$ (eV)	$\omega$ (eV)	P (D)
$Q_0$	11.108	13.802	2.693	1.347	0.743	12.455	57.595	0.008
$Q_1$	11.085	15.205	4.120	2.060	0.485	13.145	41.942	0.002
$Q_2$	4.729	9.514	4.784	2.392	0.418	7.122	10.600	0.003
$Q_3$	-14.234	-1.587	12.647	6.324	0.158	7.911	4.948	0.000

While HOMO energy is related to the ionization potential, LUMO energy corresponds to the electron activation. The energy difference between HOMO and LUMO, often referred to as the energy band gap ( $\Delta E = E_{LUMO} - E_{HOMO}$ ), is a crucial parameter that influences the stability of these molecular structures. The highest occupied molecular orbital (HOMO) is located mainly on the oxygen atoms, and the LUMO is concentrated on the vanadium atoms. The significant energy gap of  $12.647 \text{ eV}$  observed between the HOMO and LUMO orbitals, in conjunction with the relatively lower value of the electrophile index of approximately  $4.948 \text{ eV}$ , indicates that the  $Q_3$  units have limited chemical reactivity from a kinetic perspective [22–23]. Meanwhile, the lower energy difference and the larger softness factor of the  $Q_0$  units suggest their role as electron donors. The chemical hardness of the  $Q_0$  unit ( $1.347 \text{ eV}$ ) is notably lower compared to the

other units. This implies that the  $Q_0$  unit exhibits less resistance to accepting or donating electronic charges compared to the  $Q_1$ ,  $Q_2$ , and  $Q_3$  units, in accordance with the energy band gap ( $\Delta E$ ) results. Additionally, the zero value of the dipole moment for the  $Q_3$  unit indicates the presence of a symmetry element within this unit. Our observations reveal also a significantly higher electrophile index for the  $Q_0$  unit ( $\omega = 57.59542 \text{ eV}$ ). However, the electrophile index values for the other units are lower than that of  $Q_0$ , indicating that the addition reaction of the  $Q_0$  unit to the  $Q_1$ ,  $Q_2$ , and  $Q_3$  ones is more favorable.

It is well-established that a chemical reaction between two reactants proceeds in a manner that maximizes the favorable interaction energy. This is controlled by the frontier molecular orbitals of the interacting species. Therefore, the HOMO-LUMO energy gap of the  $Q_0$  unit and other units is equally significant. A smaller energy gap between

the HOMO of the electron donor and the LUMO of the electron acceptor indicates a stronger interaction between the orbitals. Our calculations showed that  $Q_0$  with HOMO value of 11.10821 eV exhibits nucleophilic character. However,  $Q_3$  unit

with comparatively lower HOMO energy were observed to have electrophilic character, as detailed in Table 2. For further clarification, the pictorial description of HOMO-LUMO energy gaps between the vanadate units is presented in Fig. 2.

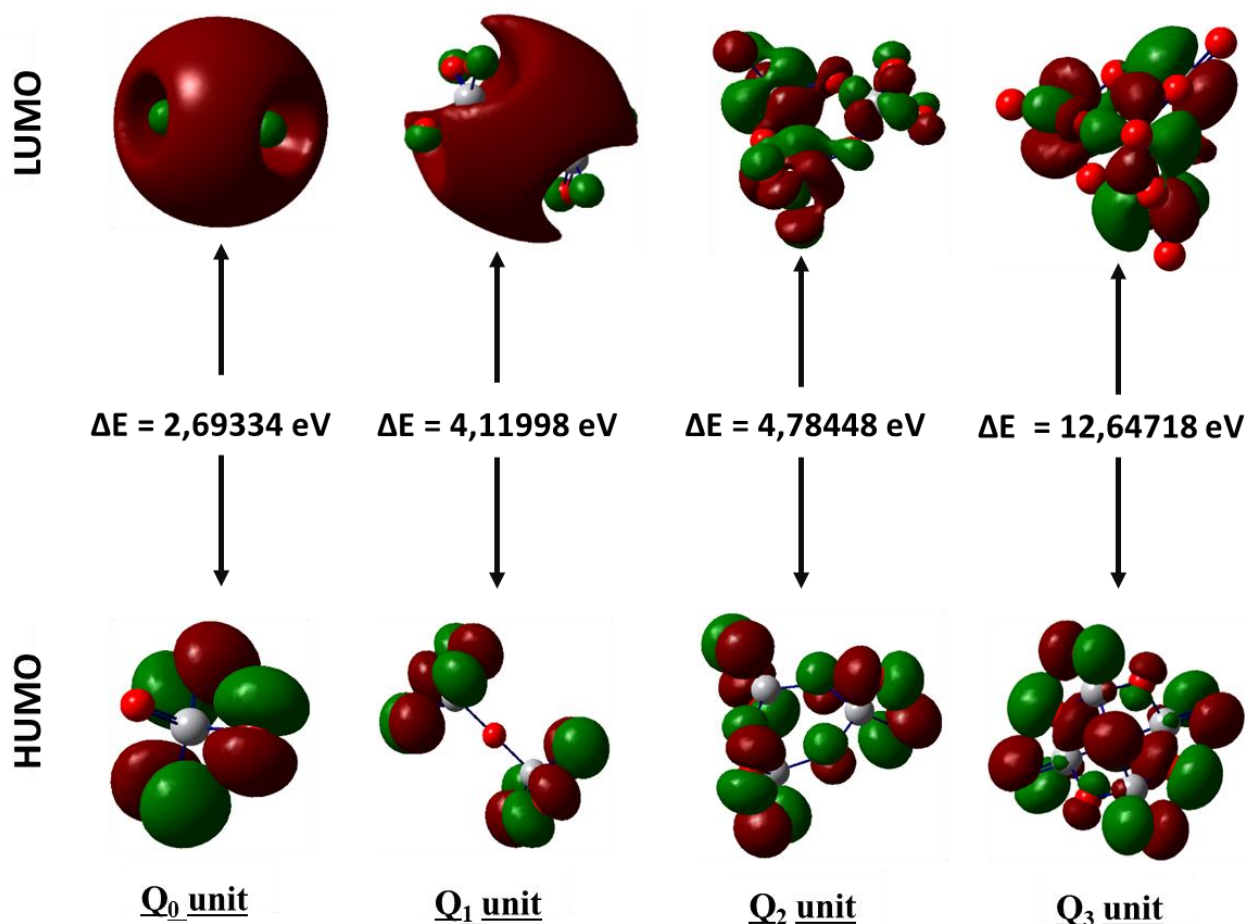


Fig. 2. Graphical representation of the frontier molecular orbital for vanadate units  $Q_0$ ,  $Q_1$ ,  $Q_2$ , and  $Q_3$ , where HOMO corresponds to the highest occupied molecular orbital and LUMO represents the lowest unoccupied molecule

The energy gap in the  $Q_3$  unit contributes to its superior stability compared to the other units. Conversely, among the various units, the  $Q_0$  vanadate units exhibit the smallest energy gap ( $\Delta E$ ) value, making them the least stable ones. The energy gap exhibits a decreasing order as follows:  $Q_3 > Q_2 > Q_1 > Q_0$ .

**Molecular electrostatic potential analysis.** Molecular electrostatic potential (MEP) mapping is used to investigate the relationships between molecular structure and physico-chemical properties [24–25]. In order to predict reactive sites for electrophilic and nucleophilic attacks on the  $Q_1$ ,  $Q_2$ , and  $Q_3$  units, Fig. 3 illustrates their respective molecular electrostatic potential

distribution. The analysis of the MEP surface represents charge distribution on the molecular surface. The colored regions on the surface aid in the identification of chemically reactive sites. Fig. 3 is the same representation in 3D dimensions of the theoretical electrostatic potential map. The negative regions (red) are related to nucleophilic reactivity of the molecule, and the positive regions (green) are preferred site for electrophilic attack [26]. The obtained results reveal the extension of the positive electrostatic potential around the vanadium atoms and the regions of negative electrostatic potential around the oxygen atoms.

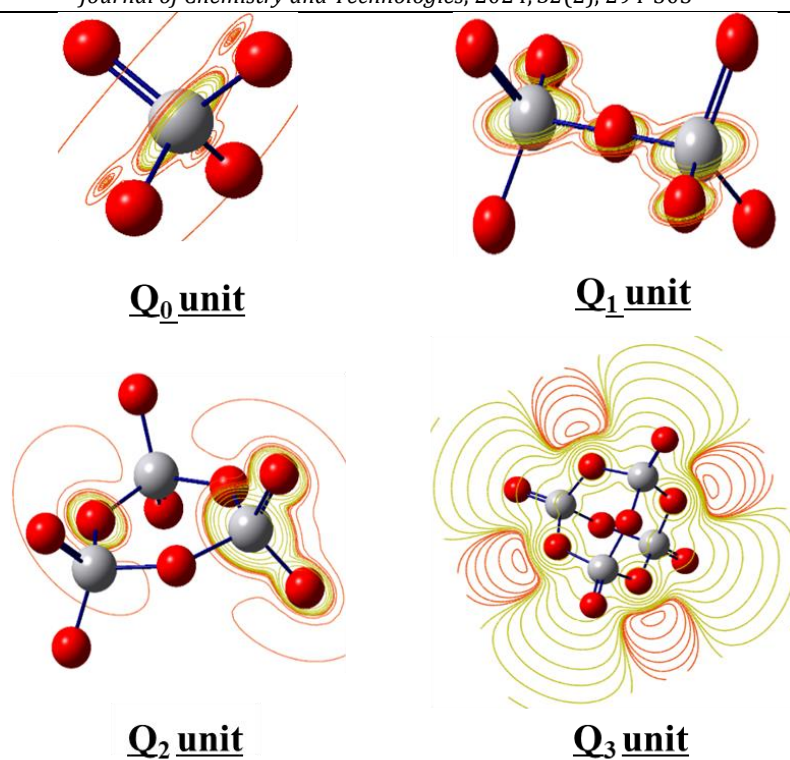


Fig. 3. Molecular electrostatic potential distribution map of Q<sub>0</sub>, Q<sub>1</sub>, Q<sub>2</sub> and Q<sub>3</sub> vanadate units

*Spectroscopic study.* Fig. 4 displays the calculated FTIR and RAMAN spectra of the various investigated vanadate units, respectively. Table 3 provides a summary of the corresponding frequencies and peak assignments. These spectra show distinct vibrational peaks related to the symmetrical deformation vibrations of the O-V-O angles in the Q<sub>0</sub> ([VO<sub>4</sub>]<sup>4-</sup>), Q<sub>1</sub> ([V<sub>2</sub>O<sub>7</sub>]<sup>4-</sup>), Q<sub>2</sub> ([V<sub>3</sub>O<sub>9</sub>]<sup>3-</sup>) and Q<sub>3</sub> ([V<sub>4</sub>O<sub>10</sub>]<sup>0</sup>) tetrahedral units [27; 28]. These peaks are notably observed within the frequency range of 350 cm<sup>-1</sup> to 650 cm<sup>-1</sup>. Additionally, symmetrical and asymmetrical stretching vibrations of the V-O bonds are

detected between 800 cm<sup>-1</sup> and 1000 cm<sup>-1</sup> [26–28]. Moreover, the symmetric and asymmetric stretching vibrations of the V-O-V bonds [26; 27] are evident in the range between 800 cm<sup>-1</sup> and 1000 cm<sup>-1</sup>. Additionally, symmetrical and asymmetrical stretching vibrations of the V-O bonds are detected at frequencies exceeding 1000 cm<sup>-1</sup> [29–31]. The spectra highlight also that the increase in bridging oxygen leads to a shift of the deformation bands towards lower frequencies and the elongation bands towards higher frequencies.

Table 3

Calculated IR and Raman active modes and frequency assignment for the Q<sub>0</sub>, Q<sub>1</sub>, Q<sub>2</sub>, and Q<sub>3</sub> vanadate units (v.w - very weak, w - weak, m - medium, s - strong, v.s - very strong)

Wavenumbers (cm <sup>-1</sup> )	IR	Raman	Assignment
<b>Q<sub>0</sub></b>			
300–500	v.w	v.w	Symmetric and Asymmetric deformation vibrations of angles O–V–O
700–900	v.s	v.s	Symmetric and Asymmetric stretching vibrations of V–O bonds
<b>Q<sub>1</sub></b>			
200–500	v.w	m	Symmetric and Asymmetric deformation vibrations of angles O–V–O
450–800	v.s	m	Symmetric and Asymmetric stretching vibrations of V–O–V bonds
800–900	v.s	v.s	Symmetric and Asymmetric stretching vibrations of V–O bonds
<b>Q<sub>2</sub></b>			
150–500	-	m	Symmetric and Asymmetric deformation vibrations of angles O–V–O
500–900	v.s	m	Symmetric and Asymmetric stretching vibrations of V–O–V bonds
900–1050	m	v.s	Symmetric and Asymmetric stretching vibrations of V–O bonds
<b>Q<sub>3</sub></b>			
200–500	v.w	m	Symmetric and Asymmetric deformation vibrations of angles O–V–O
500–1000	v.s	v.w	Symmetric and Asymmetric stretching vibrations of V–O–V bonds
1100–1350	s	v.s	Symmetric and Asymmetric stretching vibrations of V–O bonds

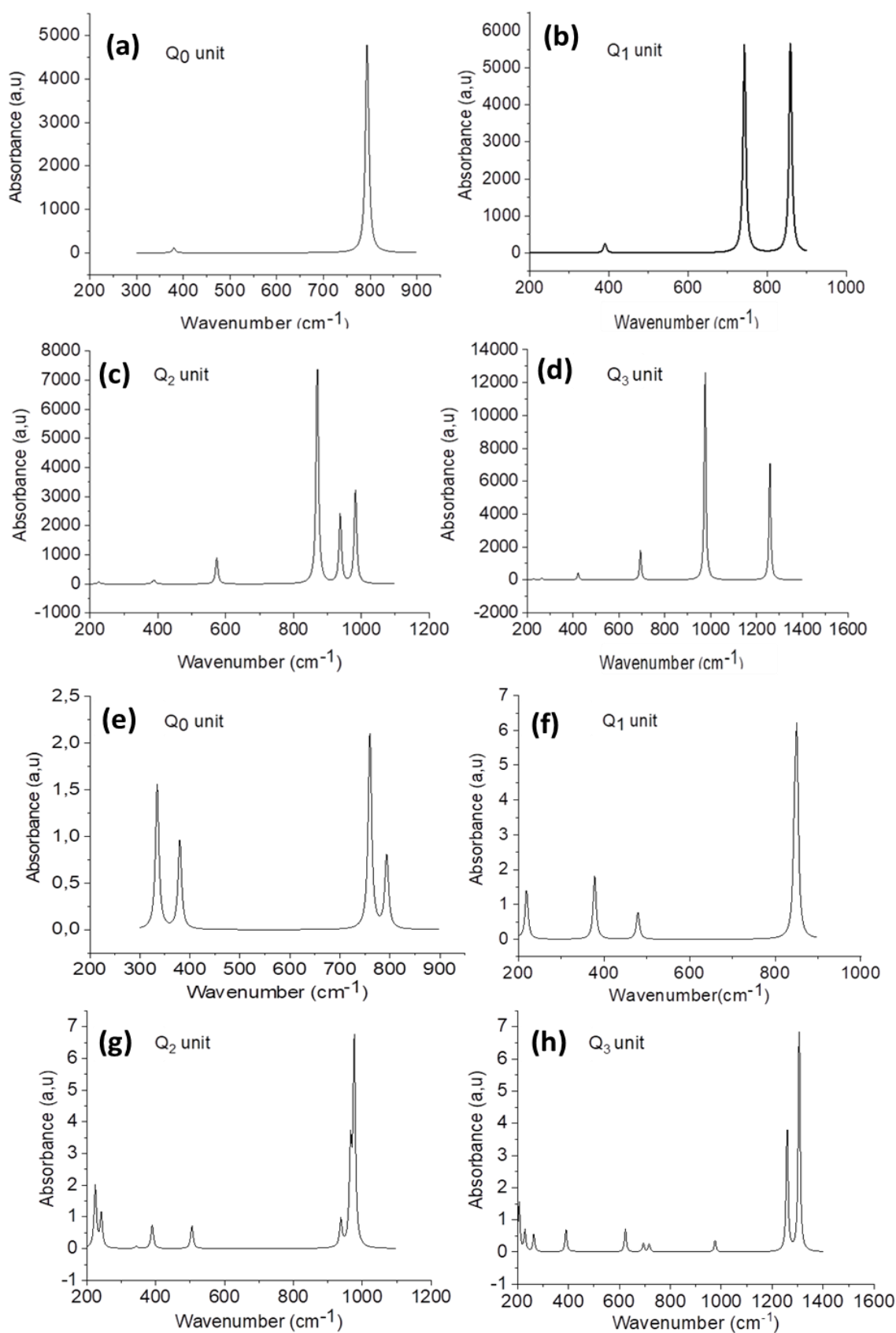


Fig. 4. Calculated FTIR (a, b, c, d) and Raman (e, f, g, h) spectra of the studied  $Q_0$ ,  $Q_1$ ,  $Q_2$ , and  $Q_3$  vanadate units

Prediction of local reactivity of reactants using FUKUI indexes for  $Q_0$ ,  $Q_1$ ,  $Q_2$ , and  $Q_3$  unit. In this current application, we determine the optimization of the previous units, using local

reactivity indices (Fukui indices). We will now elucidate how this process enables the integration of unit  $Q_0$  as an electron donor into another unit.

In this part of this study, we will examine the reactivity of the Q<sub>1</sub>: ([V<sub>2</sub>O<sub>7</sub>]<sup>4-</sup>), Q<sub>2</sub>: ([V<sub>3</sub>O<sub>9</sub>]<sup>3-</sup>), Q<sub>3</sub>: ([V<sub>4</sub>O<sub>10</sub>]<sup>0</sup> vanadate units, exhibiting the highest reactivity with the Q<sub>0</sub> ([VO<sub>4</sub>]<sup>3-</sup>) ones to form a stable structured product and identify the electrophilic sites conductive, using local reactivity indices (Fukui indices).

Local Fukui functions are tools that are useful for assessing the reactivity of various sites in the vanadate units for nucleophilic  $f_K^+$  and electrophilic  $f_K^+$  attacks [32].

Expressions for these parameters were proposed:

For a nucleophilic attack:

$$f_K^+ = [q_K(N + 1) - q_K(N)]. \quad (7)$$

For an electrophilic attack:

$$f_K^- = [q_K(N) - q_K(N - 1)], \quad (8)$$

where  $q_K(N)$ ,  $q_K(N + 1)$ , and  $q_K(N - 1)$  correspond the electron population of the K atom in the neutral, anionic, and cationic molecule, respectively. The Fukui index  $f_K^+$  measures the susceptibility of an electronic site to act as an

electron donor. Electronic sites with large positive Fukui indices have a higher probability of reacting with electron acceptors, such as vacant sites or electrophiles. However, the Fukui index  $f_K^-$  measures the susceptibility of an electronic site to act as an electron acceptor. Electronic sites with large negative Fukui indices have a higher probability of reacting with electron donors, such as nucleophiles. The obtained Fukui indices values are listed in Table 4. Notably, the vanadium atoms within units Q<sub>1</sub>, Q<sub>2</sub>, and Q<sub>3</sub> exhibit considerably higher  $f_K^-$  values. In contrast, the Q<sub>0</sub> unit displays characteristics associated with nucleophilic behavior, as evidenced by its  $f_K^+$  values. This implies that the most reactive sites, as indicated by the second-order Fukui indices ( $f_K^2$ ), have values below zero [33]. This observation suggests that these sites are more inclined to act as favorable electrophiles, making them potential candidates for interacting with the Q<sub>0</sub> unit.

Table 4

Values of the FUKUI INDICES of a: Q<sub>0</sub> unit", b: Q<sub>1</sub> unit ", c: Q<sub>2</sub> unit " and d: Q<sub>3</sub> unit"

Unit	Atoms	V <sub>1</sub>	O <sub>2</sub>	O <sub>3</sub>	O <sub>4</sub>	O <sub>5</sub>									
a- Q <sub>0</sub>	$f_K^+$	-0.79	-0.04	-0.06	-0.06	-0.06									
	$f_K^-$	-0.05	-0.16	-0.30	-0.30	-0.30									
	$f_K^2$	-0.83	0.12	0.24	0.24	0.24									
Unit	Atoms	V <sub>1</sub>	V <sub>2</sub>	O <sub>3</sub>	O <sub>4</sub>	O <sub>5</sub>	O <sub>6</sub>	O <sub>7</sub>	O <sub>8</sub>	O <sub>9</sub>					
b- Q <sub>1</sub>	$f_K^+$	-0.46	-0.46	-0.01	-0.01	-0.03	-0.01	-0.01	-0.01	-0.01	-0.12				
	$f_K^-$	0.00	0.00	-0.10	-0.19	-0.19	-0.05	-0.19	-0.09	-0.19					
	$f_K^2$	-0.46	-0.46	0.09	0.18	0.16	0.04	0.18	0.09	0.07					
Unit	Atoms	V <sub>1</sub>	V <sub>2</sub>	V <sub>3</sub>	O <sub>4</sub>	O <sub>5</sub>	O <sub>6</sub>	O <sub>7</sub>	O <sub>8</sub>	O <sub>9</sub>	O <sub>10</sub>	O <sub>11</sub>	O <sub>12</sub>		
c- Q <sub>2</sub>	$f_K^+$	-0.02	-0.02	-0.04	-0.11	-0.17	-0.05	-0.05	-0.12	-0.12	-0.06	-0.12	-0.12		
	$f_K^-$	0.01	0.01	0.02	-0.02	-0.11	-0.06	-0.06	-0.20	-0.14	-0.06	-0.20	-0.14		
	$f_K^2$	-0.04	-0.04	-0.04	-0.09	-0.06	0.01	0.01	0.08	0.02	-0.00	0.08	0.02		
Unit	Atoms	V <sub>1</sub>	V <sub>2</sub>	O <sub>3</sub>	O <sub>4</sub>	O <sub>5</sub>	O <sub>6</sub>	O <sub>7</sub>	O <sub>8</sub>	O <sub>9</sub>	O <sub>10</sub>	O <sub>11</sub>	O <sub>12</sub>	V <sub>13</sub>	O <sub>14</sub>
d- Q <sub>3</sub>	$f_K^+$	-0.03	-0.03	-0.05	-0.14	-0.06	-0.03	-0.14	-0.05	-0.05	-0.06	-0.14	-0.05	-0.03	-0.14
	$f_K^-$	0.01	0.01	-0.08	-0.15	-0.05	0.01	-0.15	-0.08	-0.08	-0.05	-0.15	-0.08	0.01	-0.15
	$f_K^2$	-0.04	-0.04	0.03	0.01.	-0.01	-0.04	0.01	0.02	0.02	-0.01	0.01	0.03	-0.04	0.01

## Conclusion

In conclusion, we have conducted a theoretical study using the Density Functional Theory (DFT) with the RB3LYP/6-311G model. The addition of a vanadate unit is found to impact the Mulliken charges within the units. Interatomic distances and angles were optimized and exploited. The electrostatic potential revealed that negative charge density is concentrated around oxygen atoms bonded to vanadium through double bonds, as well as bridging oxygen (BO). Various parameters, such as HOMO and LUMO energies, energy difference ( $\Delta E$ ), chemical hardness, chemical potential, softness, and overall electrophilicity index have been thoroughly investigated. Simulated FTIR and RAMAN spectra

indicated a shift in the symmetrical and asymmetrical vibrational bands in the studied units as a function of the number of vanadate units. The possibility of forming a stable chain of the vanadate product via Q<sub>0</sub> ([VO<sub>4</sub>]<sup>4-</sup>) ions to other vanadate units has been also investigated. In this context, the vanadate units (Q<sub>1</sub>, Q<sub>2</sub>, and Q<sub>3</sub>) act as electron acceptors while the isolated ([VO<sub>4</sub>]<sup>4-</sup>) ion behaves as an electron donor. Vanadium atoms within certain units (Q<sub>1</sub>, Q<sub>2</sub>, and Q<sub>3</sub>) demonstrate notably elevated values, whereas the Q<sub>0</sub> unit exhibits characteristics commonly associated with nucleophilic behavior. It is suggested that sites with second-order Fukui indices below zero are predisposed to act as

advantageous electrophiles, potentially leading to interactions with the  $Q_0$  unit.

### Acknowledgments

This research did not receive any specific grant from funding agencies in the public, commercial, or not-for profit sectors.

### Author contribution instruction

A. EL Addali: Conceptualization, Investigation and Writing – original draft; A. EL Boukili: Conceptualization, Supervision and Writing –

review & editing; L. Boudad: Conceptualization, Investigation and Writing – review & editing; H. Zouihri: Writing – review & editing; M. Taibi: Investigation, Supervision and Writing – review & editing; T. Guedira: Investigation and Supervision

### Declaration of competing interest

The authors declare that they have no known competing financial interests or personal relationships that could have appeared to influence the work reported in this paper.

### References

- [1] Lee, J. C., Kim, E. Y., Chung, K. W., Kim, R. H., Jeon, S. (2021). A review on the metallurgical recycling of vanadium from slags: towards a sustainable vanadium production. *J. Mater. Res. Technol.*, 12, 343–364. <https://doi.org/10.1016/j.jmrt.2021.02.065>
- [2] Wachs, I. E. (2013). Catalysis science of supported vanadium oxide catalysts. *Dalton Trans.*, 42(33), 11762–11769.
- [3] Lourenssen, K., Williams, J., Ahmadpour, F., Clemmer, R., Tasnim, S. (2019). Vanadium redox flow batteries: A comprehensive review. *J. Energy Storage*, 25, 100844. <https://doi.org/10.1016/j.est.2019.100844>
- [4] Liu, K. Lee, S. Yang, S., Delaire, O., Wu, J. (2018). Recent progresses on physics and applications of vanadium dioxide. *Mater. Today*, 21(8), 875–896. <https://doi.org/10.1016/j.mattod.2018.03.029>
- [5] Muroga, T., Chen, J. M., Chernov, V. M., Kurtz, R. J., Le Fleum, M. (2014). Present status of vanadium alloys for fusion applications. *J. Nucl. Mater.* 455(1-3), 263–268.
- [6] Scibior, A., Pietrzyk, L., Plewa, Z., Skiba, A. (2020). Vanadium: risks and possible benefits in the light of a comprehensive overview of its pharmacotoxicological mechanisms and multi-applications with a summary of further research trends, *Journal of Trace Elements in Medicine and Biology*. 61, 126508. <https://doi.org/10.1016/j.jtemb.2020.126508>
- [7] Menictas, C., Skyllas-Kazacos, M. (2011). Performance of vanadium-oxygen redox fuel cell. *J. Appl. Electrochem.* 41, 1223–1232.
- [8] Skyllas-Kazacos, M., Kazacos, G., Poon, G., Verseema, H. (2010). Recent advances with UNSW vanadium-based redox flow batteries. *Int. J. Energy Res.* 34(2), 182–189.
- [9] Webster, S., Czerw, R., Nesper, R., DiMaio, J., Xu, J. F., Ballato J., Carroll, D. L. (2004). Optical properties of vanadium oxide nanotubes. *J. Nanosci. Nanotechnol.* 4(3), 260–264. [doi: 10.1166/jnn.2004.035](https://doi.org/10.1166/jnn.2004.035)
- [10] Sindhu, S., Sanghi, S. A. Agarwal, Seth Sonam, V. P. Kishore, N. (2005). The role of  $V_2O_5$  in the modification of structural, optical and electrical properties of vanadium barium borate glasses. *Phys. B: Condens. Matter.* 365, 65.
- [11] Lakshmikantha, R., Ayachit, N.H., Anavekar, R. V. (2014). Optical, physical and structural studies of vanadium doped  $P_2O_5$ - $BaO$ - $Li_2O$  glasses, *Journal of Physics and Chemistry of Solids* 75 168–173.
- [12] Khattak, G. D., Tabet, N., Wenger, L. E. (2005). Structural properties of glasses in the series  $(SrO)_x(V_2O_5)_{1-x}$ ,  $(SrO)_{0.5-y}(B_2O_3)_y(V_2O_5)_{0.5}$ , and  $(SrO)_{0.2}(B_2O_3)_z(V_2O_5)_{0.8-z}$ . *Phys. Rev. B*, 72, 104203.
- [13] Brow, R. K. Non-Cryst. J. (2000). The structure of simple phosphate glasses. *Solids*, 263-264, 1–28.
- [14] Ehrt, D. (2015). Phosphate and fluoride phosphate optical glasses — properties, structure and applications, *Phys. Chem. Glasses: Eur. J. Glass Sci. Technol. B*, 56(6), 217–234.
- [15] Frisch, M. J., Trucks, G. W., Schlegel, H. B., Scuseria, G. E., Robb, M. A., Cheeseman J. R. (2009). *Gaussian 09 revision C, 1. Gaussian Inc*, Wallingford C.T.
- [16] Khan, M. F. R., Rashid, B., Rahman, M. M., Al Faruk, M. M., Rahman, M., Rashid, M. A. (2017). Effects of solvent polarity on solvation free energy, dipole moment, polarizability, hyperpolarizability and molecular reactivity of aspirin. *Int. J. Pharm. Pharm. Sci*, 9(2), 217–221
- [17] Vijayakumar, S., Kolandaivel, P. (2006). Study of static dipole polarizabilities, dipole moments, and chemical hardness for linear  $CH_3-(CC) n-X$  ( $X = H, F, Cl, Br$ , and  $NO_2$  and  $n = 1-4$ ) molecules. *J. Mol. Struct. Theochem.* 770(1-3), 23–3.
- [18] Afzal, Q. Q., Jaffar, K., Ans, M., Rafique, J., Iqbal, J., Shehzad, R. A., Mahr, M. S. (2022). Designing benzothiadiazole based highly efficient non-fullerene acceptor molecules for organic solar cells. *Polymer*, 238, 124405. <https://doi.org/10.1016/j.polymer.2021.124405>
- [19] Valero-Romero, M. J. Cabrera-Molina, A. Gomero-Pérez, M. O Rodriguez-Mirasol J., Cordero, T. (2014). *Catalysis Today*, 233–241.
- [20] Dasireddy, V. D. B. C., Singh S., Friedrich, H. B. (2012). *Applied Catalysis A: General*, 421-422, 58–69.
- [21] Cheng, L. Ferguson, G. L. Zygmunt S. A., Curtiss, L. A. (2013). *Journal of Catalysis*, 302, 31–36.
- [22] Buyukuslu, H., Akdogan, M., Yildirim, G., Parlak, C. (2010). Ab initio Hartree-Fock and density functional theory study on characterization of 3-(5-methylthiazol-2-ylidiazenyl)-2-phenyl-1H-indole. *Spectrochim. Acta A*, 75, 1362.
- [23] Parr, R., Szentpaly, L., Liu, S. (1999). Electrophilicity index. *J. Am. Chem. Soc.*, (121) 1922.
- [24] Lipkowitz, K. B., Boyd, D. B. (2009). *Reviews in Computational Chemistry, Vol. 5*, John Wiley & Sons.
- [25] Naray-Szabo, G., Ferenczy, G. (1995). Molecular electrostatics. *Chem. Rev.* 95, 829.
- [26] Nataraj, A., Balachandran, V., Karthick, T. (2013). Molecular orbital studies (hardness, chemical potential, electrophilicity, and first electron excitation), vibrational investigation and theoretical NBO analysis of 2-hydroxy-5-bromobenzaldehyde by density functional method. *J. Mol. Struct.*, 1031, 221–233.
- [27] Guo, H. W., Wang, X. F., Gong, Y. X., Gao D. N. (2010). Mixed alkali effect in  $xK_2O-(30-x) Na_2O-30P_2O_5-40ZnO$  glasses. *J Non Cryst Solids*. 356, 2109–2113.
- [28] Ternane, R., Ferid, M., Guyot, Y. Malika, T. A., Boulon, G. (2008). Spectroscopic properties of  $Yb^{3+}$  in  $NaYbP_2O_7$

- diphosphate single crystals. *J Alloys Comp.*, 464, 327–331.
- [29] Abid, M., Et-tabirou, M., Hafid, M. (2001). Glass forming region, ionic conductivity and infrared spectroscopy of vitreous sodium lead mixed phosphates. *Mater. Res. Bull.*, 36, 407–421.
- [30] Bet-thet, P., Bretey, E., Berthon J., d'Yvoire, F., Belkebir, A., Rulmont, A., Gilbert, B. (1994). Structure and ion transport properties of  $\text{Na}_2\text{O Ga}_2\text{O}_3 \text{P}_2\text{O}_5$  glasses. *Solid State Ionics*, 70/71, 476–481.
- [31] Mandlule, A., Döhler, F., VanWüllen, L., Kasuga, T., Brauer, D. S. (2014). Changes in structure and thermal properties with phosphate content of ternary calcium sodium phosphate glasses. *J. Non Cryst. Solids*, 392–393, 31–38.
- [32] Vanasundari, K., Balachandran, V., Kavimani, M., Narayana, B. (2017). Spectroscopic investigation, vibrational assignments, Fukui functions, HOMO-LUMO, MEP and molecular docking evaluation of 4 – [(3, 4 – dichlorophenyl) amino] 2 – methylidene 4 – oxo butanoic acid by DFT method, *Journal of Molecular Structure*, 1147, 136–147.
- [33] Haldhar, R., Prasad, D., Mandal, N., Benhiba, F., Bahadur, I., Dagdag, O. (2021). Anticorrosive properties of a green and sustainable inhibitor from leaves extract of Cannabis sativa plant: Experimental and theoretical approach. *Colloids Surf. A: Physicochem. Eng.* 614, 126211. <https://doi.org/10.1016/j.colsurfa.2021.126211>